Received: 10 November 2021 | Revised: 31 May 2022 | Accepted: 6 June 2022

DOI: 10.1002/hyp.14634

RESEARCH ARTICLE

WILEY

Hydrological monitoring of a slope covered by stratified pyroclastic deposits and analysis of infiltration processes

Giovanna Capparelli | Gennaro Spolverino

Dipartimento di Ingegneria Informatica, Modellistica, Elettronica e Sistemistica, Università della Calabria, Rende, Italy

Correspondence
Gennaro Spolverino, Università della Calabria, via P. Bucci, 87036 Rende (CS), Italy.
Email: g.spolverino@dimes.unical.it

Funding information
Framework of the SILA—PONa3_00341 project

Abstract

In addition to the duration and intensity of rainfall, infiltration processes are strongly affected by the hydraulic properties of the soil. In the case of heterogeneous and stratified soil profiles, the analysis of the infiltration process becomes more complex, since conflicting hydraulic properties of adjacent layers can induce locally diverted flow. Soils of volcanic origin present these characteristics, because during the various eruptive phases, layers with very different textures are deposited. In this article, data are analysed which have been recorded by a monitoring station installed on a slope made up of volcanic deposits. The station consists of a rain gauge to measure rainfall and seven tensiometers and eight TDR probes installed at different depths to measure suction and volumetric water content, respectively. The slope is made up of alternating volcanic ash (silt-sandy-clay paleosoils) interspersed with pumice (sandy-gravel), due to the different eruptive phases of the volcanic complexes in the area. The analysis of the data established that the layers of coarser material (pumices), depending on the initial moisture conditions, may hinder or even favour the infiltration of water into the deeper layers. In particular, when water content is low, the pumices presented a low unsaturated conductivity which hindered infiltration. By contrast, in wetter conditions, they favoured the flow of water. Therefore, the initial moisture conditions of the soil layers must be taken into account for a correct prediction of the infiltration phenomena. Dry conditions of the pumice layers can hinder drainage into the lower layers, thus favouring the rapid accumulation of soil water during rainfall events, which could eventually lead to slope failure.

KEYWORDS
capillary barrier, infiltration, in-situ measurements, layered soil, pyroclastic deposits

1 | INTRODUCTION

The prediction of natural processes, such as precipitation-induced landslides, is a problem of great importance. Every year, meteorological events trigger surface and deep landslides on slopes, which cause considerable damage and reap victims. In order to understand the processes underlying the triggering of a landslide phenomenon and to improve forecasting systems, a great deal of research has been carried out. Hydraulic disciplines such as seepage analysis and soil water circulation processes play a decisive role in understanding the processes that cause rain-induced subsidence. (Bogaard & Greco, 2016; Capparelli et al., 2020; de Luca & Capparelli, 2022; Spolverino et al., 2019; von

Ruette et al., 2014; Wieczorek & Glade, 2005). The hydrogeological response of the groundwater regime to the triggering of deep-seated landslides is strongly correlated to the history of prior rainfall (Lv et al., 2019; Padilla et al., 2014). Rain-induced surface landslides usually occur along slopes covered by granular deposits, in saturated or unsaturated conditions, as a result of an increase in interstitial water pressure. Deposit-covered slopes with an inclination greater than the angle of friction of soils and reduced cohesion are stable due to the contribution to soil shear resistance made by matrix suction in unsaturated conditions. (e.g., Fredlund & Morgenstern, 1977; Greco & Gargano, 2015; Lu et al., 2010; Vanapalli et al., 1996; Wheeler et al., 2003). Rain-induced landslides are triggered by a reduction in suction due to an increase in water content. (e.g., Baum et al., 2010; Collins & Znidarcic, 2004; Damiano & Olivares, 2010; Greco et al., 2013; Lu & Godt, 2008). In the simple case of a regular geometry slope, with homogeneous and isotropic covering, the direction of the infiltration flow is orthogonal to the ground plane whenever the capillary gradient dominates (i.e., in unsaturated conditions), whilst it becomes vertical when, approaching saturation, the flow tends to be guided by gravity (e.g., Lu et al., 2011). In the case of heterogeneous and stratified soil profiles, the analysis of the infiltration process becomes more complex, as the conflicting hydraulic properties of adjacent layers can provoke locally diverted flow. (e.g., Formetta & Capparelli, 2019; Hübner et al., 2017; Ross, 1990; Schneider et al., 2014; Warrick et al., 1997; Yang et al., 2006).

The studied area is a portion of the Mount Pizzo d'Alvano, in Campania, (southern Italy). This area was affected by a catastrophic series of debris flows on 5–6 May 1998 that resulted in the loss of 152 lives. Following these events, hydrological monitoring activities were carried out on the slope, installing a monitoring station to measure rainfall, water content and matrix suction at different depths. The field data allowed distinguishing seasonal fluctuations in suction related to the long-term or short-term response to meteorological forces (Cascini et al., 2014; Comegna et al., 2016). This article deals with the hydrological behaviour of a slope covered by layered granular pyroclastic deposits, usually in unsaturated conditions, consisting mainly of ash and pumice, resting on fractured limestone. Detailed knowledge of the hydrological processes that involve unsaturated pyroclastic deposits in response to meteorological forces is important to better understand the mechanisms regulating infiltration processes in soils formed by several layers with very different grain sizes.

The aim of the work is to analyse and discuss the hydrological processes involving the slope of Mount Pizzo d'Alvano. The mountain is covered by pyroclastic deposits, consisting of alternating layers of unsaturated volcanic ash and pumice, with outcrops of carbonate rocks. This deposit is the result of various eruptive phases of the Somma-Vesuvius volcano and the Campi Flegrei and others that are no longer active. (Rolandi et al., 2003; Sorbino & Nicotera, 2013). The phenomena observed along these areas are strongly influenced by unsaturated coverings. As reported in Damiano and Olivares (2010), this mountain is characterised by steep slopes (angle of inclination greater than the angle of friction of the soil); the flows occur essentially in shallow and cohesionless deposits in primary deposition lying on fractured limestone; the water table is absent and the deposits are initially unsaturated. Several studies have investigated how stratification affects the process of infiltration through volcanoclastic coverings in Campania and the possible triggering of landslides. (Capparelli et al., 2020; Cascini, Ferlisi, & Vitolo, 2008; Damiano et al., 2017; Damiano & Olivares, 2010; Mancarella et al., 2012). Although a number of authors have argued that in some cases pumices can act as a capillary barrier, through which water can only pass if a critical value of water potential is reached (Ross, 1990; Stormont & Anderson, 1999), the behaviour of layered pyroclastic soils during infiltration is more complex, as it depends on the initial moisture conditions and the infiltration rate. Our specific objectives were:

i. to analyse infiltration processes during one hydrological years (2015–2016) using in-situ measurements of volcanic layered soils,
ii. to develop experimental water retention curves and permeability functions of the pyroclastic ash and
iii. to evaluate the role of pumice layers as capillary barriers on infiltration processes.

2 | DATA AND METHODS

2.1 | Experimental site and monitoring station

The instability of pyroclastic soils is one of the most topical and catastrophic problems involving the Campania region (southern Italy). In this area, several volcanic eruptions of large complexes, that is, Somma-Vesuvius, Campi Flegrei and Roccamonfina, have occurred over the last 40 000 years (Di Crescenzo & Santo, 2005; Rolandi et al., 2003). The resulting materials are spread over a large area around the city of Naples and the slope coverings are often subject to rain-induced landslides. (e.g., Cascini, Cuomo, & Guida, 2008; Di Martire et al., 2012; Revellino et al., 2008). In recent years, the scientific community has been urged to study and investigate the instability of soils of pyroclastic origin covering the slopes around the Vesuvius area (Naples, Italy), in particular the Pizzo d'Alvano ridge, especially following the tragic landslide events of 5–6 May 1998 which killed 152 people.

The stratigraphy of this area is extremely variable. (de Vita et al., 2006; de Vita et al., 2018; del Prete et al., 1998; del Soldato et al., 2018). Generally speaking, the deposits are incoherent, varying in grain size from sands, silty sands and silts (ashes) to gravels and sands with gravels (pumices). In particular, the ashes show a rather variable degree of compaction, with porosity ranging between 0.5 and 0.75 (Sorbino & Nicotera, 2013). Along the slopes, the hydrogeological characteristics of the pyroclastic deposits are mainly linked to the continuity of the ash and pumice layers which affect the rainfall infiltration process. These slopes have undergone significant modelling during the cold, glacial and stadial climatic phases, and this has produced large quantities of foothill debris, within which pyroclastic

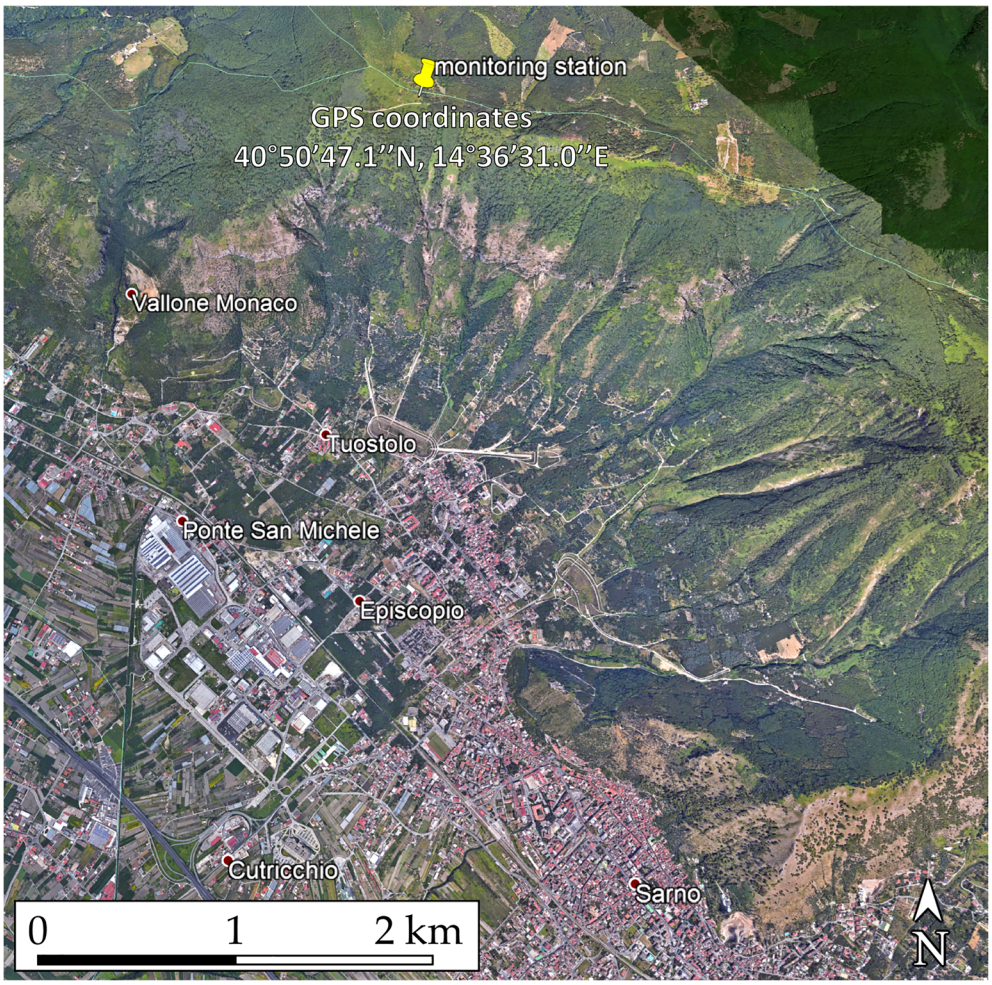

FIGURE 1 Position of monitoring station

components linked to the ancient Vesuvian and Phlegraean eruptive events are to be found. Such modelling has produced morphological concavities, with the creation of rectilinear valleys, which form the so-called "Zero Order Basin" (hereafter ZOB).

The events of May 1998 are considered to be localised first-detachment landslides, which affected the summit portions of the ZOBs.

In the described area, the decision was taken to install a monitoring station to study the infiltration processes responsible for triggering landslides. The station was installed in particular geological-stratigraphic and geomorphologic conditions. Specifically, the monitored site is located in a morphological concavity (ZOB), situated in the upper part of the slope of Pizzo d'Alvano, near the relief known as "Torre Savaio" and close to some of the landslides which occurred in May 1998 in Sarno (Figure 1).

From the ECMWF data, the average annual rainfall is 1143 mm. The driest month is July, with 18 mm of rain. The month of November is the one with the most rain, having an average of 190 mm. This site is of particular interest because it represents an area that was not affected by the landslide events of May 1998 at Sarno; in fact the ZOB did not empty and represents, with good approximation, the pre-event hydrogeological conditions.

The monitoring station consists of seven tensiometers and eight time domain reflectometry (TDR) probes at different depths to measure suction ψ and volumetric water content θ, respectively. TDR is a widely used indirect technique for field measurements of soil water content. (Jones et al., 2002), providing soil dielectric permittivity values, ε_r, which can be related to the volumetric water content of the soil, θ, through specific calibration expressions (Capparelli et al., 2018; Topp et al., 1980). The sensors continuously record the state of the soil, taking systematic measurements every minute. The data is sent to a data logger at 10-min intervals and can be downloaded directly on site or from a remote server. In addition to the sensors monitoring the ground conditions, a tilting rain gauge was installed to record rainfall events at the site. The station uses electricity from a battery which is recharged by a solar panel. The installation of the station was preceded by the construction of a hand dug trench, approximately 2 m wide and 2 m deep. The TDR probes were pushed horizontally into its walls at various depths. At the points where they emerged from the ground, the sensors were protected by concrete manholes. The cables were routed through a spiral pipe, which in turn was protected by a double-walled cable duct. The cable entrances in the manholes were cemented and the manholes were closed with rock wool to prevent small animals from entering. At the bottom of the manholes, which are perforated to allow rainwater to drain away, is a layer of gravel

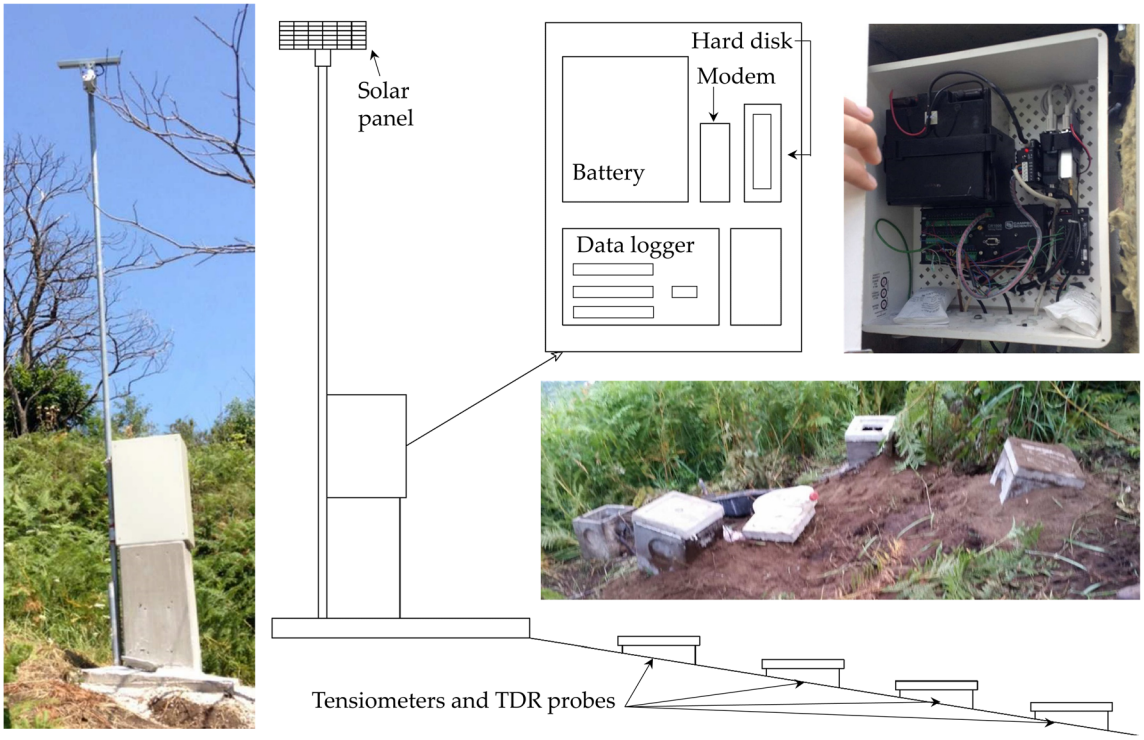

FIGURE 2 Monitoring station layout

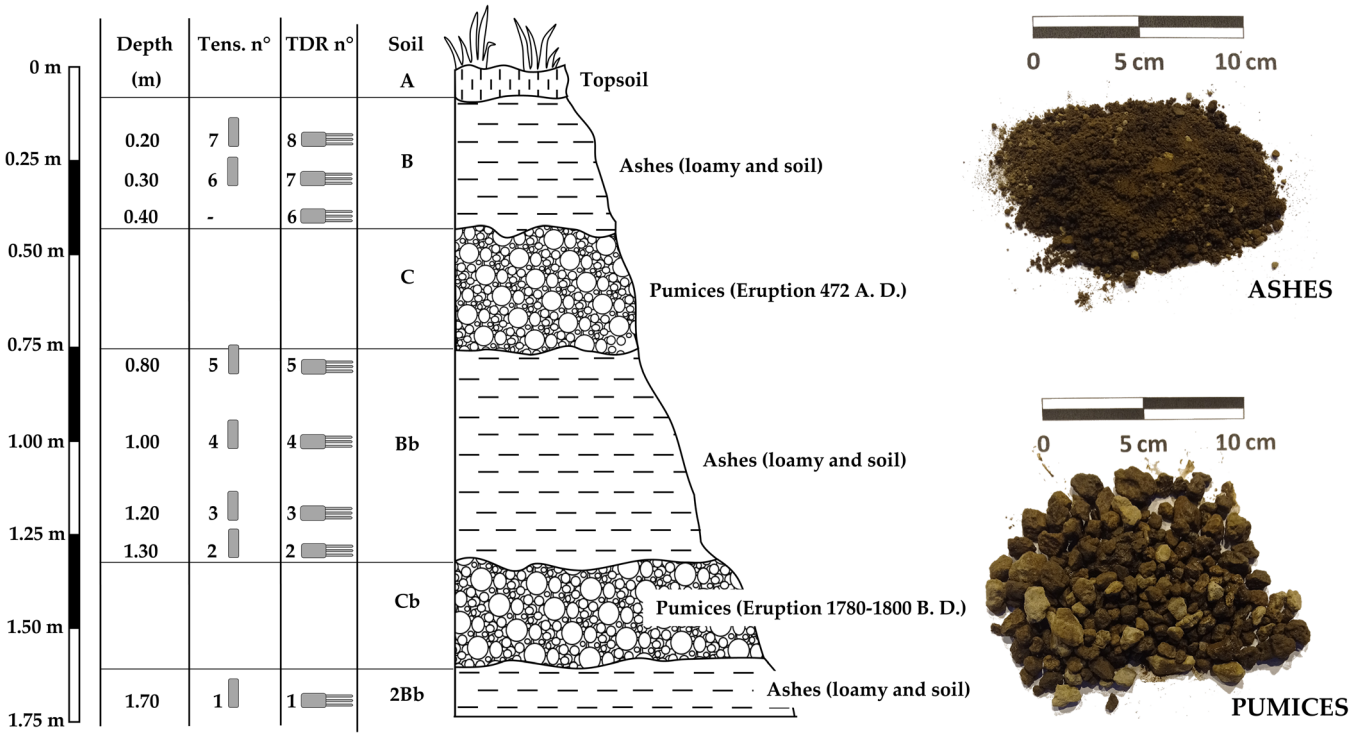

FIGURE 3 Stratigraphy observed on site and position of sensors (modified after Capparelli & Spolverino, 2020). Images of the pumice and ash layers

to prevent stagnation. The main container of the station was fixed to the ground to prevent tampering. The cables to the solar panel and communication antenna were protected in a thick metal tube; the antenna and panel were installed approximately 5.5 m above the ground to prevent tampering and minimise fire damage. The diagram of the monitoring station is shown in Figure 2.

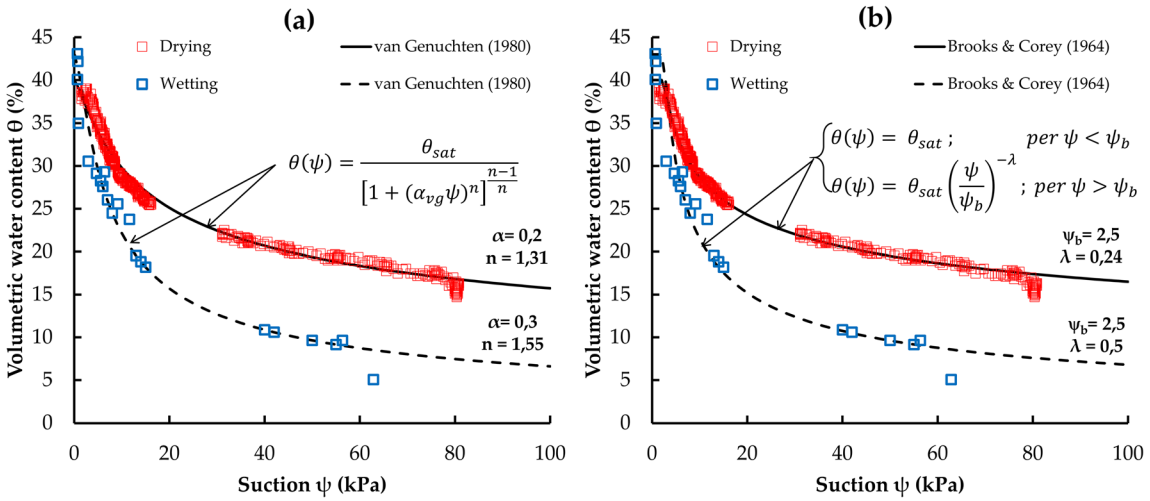

FIGURE 4 Water retention curves in the infiltration and evaporation phases. (a) Model of Van Genuchten (1980). (b) Model of Brooks and Corey (1964). (modified after Capparelli & Spolverino, 2020)

Direct investigations carried out on site (exploratory pits and trenches) delineated the stratigraphy and thicknesses of the pyroclastic blanket, recognising the alternation of sandy-gravelly pumices interspersed with silt-sandy-clay cineritic palaeosols. The stratigraphy and the levels affected by the installation of the sensors are schematically shown in Figure 3, which also includes images of the ash and pumice layers.

2.2 | Soil properties

The volcanic ash present in the installation area of the monitoring station has a specific grain weight (*G*) of about 2.6 g/cm^3 and a porosity (*n*) of about 68% according to Olivares et al. (2019). Whilst the pumices have a specific grain weight ranging between 2.4 and 2.5 g/cm^3 and a porosity between 30% and 42% according to Basile et al. (2003) and de Vita et al. (2013). By means of laboratory tests, the particle size class of the ashes was defined (Capparelli et al., 2018). The soils analysed are clayey sands.

The water retention curve (SWRC) of the ash layers was also defined (Capparelli & Spolverino, 2020). A TDR probe for measuring volumetric water content and a tensiometer for measuring suction were installed inside a cylindrical sample of pyroclastic ash with a diameter of 33 cm and a thickness of 6 cm.

Following the installation of the sensors, an imbibition phase was initiated by providing water spray from above. The water was sprayed with a manual nebuliser on the upper surface (8.55 dm^2) and the test ran for 1 h 40 min. Water volume supplied was approximately 3 L, which is equivalent to a rainfall intensity of 22 mm/h and which is coherent with the porosity of the sample.

During the entire phase, the wet front and the suction value were monitored. The test continued until we were certain that the deposit was completely saturated, that is, that the wet front had reached the base of the soil and that suction was close to zero. After water supply stopped, the drying phase began, leaving the deposit to evaporate naturally.

The experimental measurements provided a series of discrete points useful for defining the relationship between suction and water content and thus for determining the formulation of the water retention curve in continuous mathematical form. The pairs of experimental values were interpolated with the mathematical relationships modelling the water retention curve. In particular, the values were interpolated using the model of van Genuchten (1980) with the simplification of Mualem (m = [n−1]/n) and the model of Brooks and Corey (1964). Both models were simplified by setting the residual water content to zero ($\theta_{res} = 0$).

Figure 4a,b shows the pairs of water content and suction values recorded at the same time, and the curves obtained by interpolating the models of van Genuchten (1980) and Brooks and Corey (1964), respectively.

As can be seen from the graphs, both models optimally interpret the experimental data. The test in the infiltration phase was carried out starting from an almost completely dry deposit and was brought to complete saturation; the test in the evaporation phase, on the other hand, started with the deposit in saturated conditions and was left to evaporate, with a tendency towards dry conditions. Given the way the test was carried out, therefore, the curves obtained represent the main imbibition and drying curves.

2.3 | Permeability coefficients

According to Darcy, the one-dimensional apparent infiltration velocity along the z-axis between two points within an unsaturated soil can be determined with Equation (1). The velocity, *v*, is therefore a function of the change in total load expressed in terms of elevation, *z*, and suction, ψ, and of the permeability coefficient, *k*, which depends on the water content, θ.

$$v = -k(\theta)\frac{\partial}{\partial z}(\psi - z) = -k(\theta)\frac{\partial \psi}{\partial z} + k(\theta). \quad (1)$$

Knowing the apparent velocity, it is possible to determine the permeability coefficient by inverting the Darcy equation (Equation (2)).

$$k(\theta) = \frac{v}{\left(1 - \frac{\partial \psi}{\partial z}\right)}. \quad (2)$$

In our case, however, we do not know the continuous trend of suction along the depth; we only have point values at the installation depths from the tensiometers. It is therefore not possible to define the derivative of suction. If, however, we assume that the suction profile along z is linear at intervals, the derivative of suction across the depth is reduced to the ratio of the differences in suction and height (Equation (3)).

$$k(\theta) = \frac{v}{\left(1 - \frac{\Delta \psi}{\Delta z}\right)}. \quad (3)$$

With k-ψ and k-θ value pairs it is possible define the soil permeability functions $k(\psi)$ and $k(\theta)$. The pairs can be interpolated with the hydraulic conductivity function model of van Genuchten–Mualem (Equation (4)).

$$k_r(\Theta) = \Theta^{\frac{1}{2}}\left[1 - \left(1 - \Theta^{\frac{1}{m}}\right)^m\right]^2; (0 < m < 1),$$

$$k_r(\psi) = \frac{\left\{1 - (\alpha\psi)^{n-1}\left[1 + (\alpha\psi)^m\right]^{-n}\right\}^2}{\left[1 + (\alpha\psi)^m\right]^{\frac{n}{2}}}; m = 1 - \frac{1}{n}. \quad (4)$$

In which, α, n, m are interpolation parameters, whilst Θ and k_r are the dimensionless water content and the relative permeability, respectively, as given in Equation (5) (in which, θ_r is residual water content, θ_{sat} is saturated water content, k_{sat}, saturated permeability). Furthermore it is possible to make a simplification, with the residual water content being zero. ($\theta_r = 0$).

$$\Theta = \frac{\theta - \theta_r}{\theta_{sat} - \theta_r}; k_r = \frac{k}{k_{sat}}. \quad (5)$$

3 | RESULTS

3.1 | Soil water retention curves

The data recorded by the monitoring station for the hydrological year extending from 1 October 2015 to 30 September 2016 were analysed and an initial screening was performed, eliminating all fields in which there were "no data" and all unreliable figures. In some fields there is no data due to an occasional interruption of the electrical supply system. The recording of unreliable data (such as negative water content values) is also likely to be attributed to electrical problems. Figure 5 shows the amount of rainfall in mm recorded by the rain gauge every 2½ days (60 h) and the trends in the degree of saturation and suction at different depths, with time intervals of 3 h, recorded by the instruments in the monitoring station. The rainfall data recorded in this year are consistent with the average precipitation in the area. The cumulative annual rainfall is 1163 mm.

In all graphs, the volumetric water contents are divided by the saturated water content, thus providing a graph according to the degree of saturation Sr. From the graphs, it can be seen that the surface layers are more affected by moisture variations during individual rainfall events, whilst the deeper layers have a seasonal variation. Pairs of suction and saturation values recorded at the same time at the same depths were correlated in order to construct the soil water retention curve. These values were interpolated with the mathematical formulation of the van Genuchten model curve. Figure 6 shows the pairs of suction and saturation degree values and the curve identified by their interpolation. The graph also shows the main imbibition and drying curves obtained from the laboratory test. The curve obtained by interpolating the on-site data lies within the hysteresis formed by the two main curves. This was to be expected, since the data used to construct the curve refer to both periods of infiltration and drying. The result, therefore, is an average water retention curve, which takes into account both imbibition and drying processes. In addition, to confirm the correctness of the experimentally constructed main water retention curves, it should be noted that these contain almost all the points obtained from the in situ monitoring data.

3.2 | Infiltration processes

In order to understand the evolution of the process of soil infiltration, three significant rainfall periods were isolated and analysed. The rainfall periods identified relate to the month of February, between February and March and the month of April. These three events were chosen because they are the ones that had significant effects, in terms of suction and water content, even in the deep layers of the slope (see Figure 5). Furthermore, these three data series had no unreliable or missing values. For each of these periods, the volumetric water content recorded by the TDR probes at the various depths was plotted and the time in which they were affected by the arrival of the wet front was identified, that is, the instant in which the curve showed a rapid increase.

Figure 7a shows the rainfall recorded every 10 min by the rain gauge installed at the site from 10 to 19 February 2016. As can be seen from the illustration, it is possible to distinguish three different rainfall events. Figure 7b–d shows the volumetric water content recorded by the TDR probes at different depths. These figures also show the instants in which the curves recorded an increase, representative of the arrival of the wet front at that depth. Since there were three rainfall events, it is possible to distinguish more than a single change in slope for each curve. In particular, the probes installed in

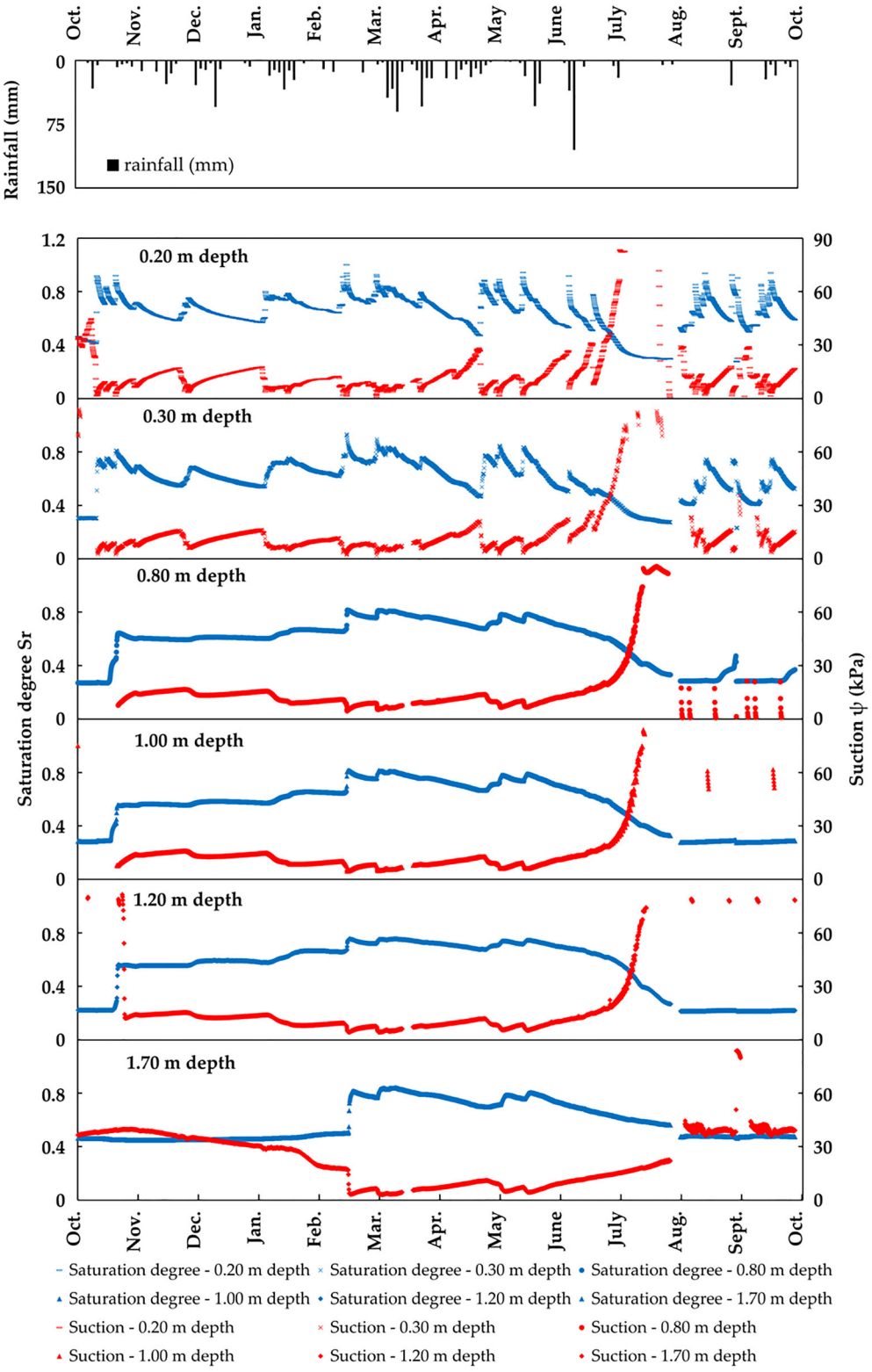

FIGURE 5 The amount of rain in mm recorded by the rain gauge every 2½ days (60 h) and the trends in the degree of saturation and suction at different depths, at 3-h intervals, recorded by the instruments in the monitoring station

the most superficial soil were affected by all three rainfall events and it was possible to distinguish three instants in which an increase was recorded. The probes installed in the second ash layer, on the other hand, recorded only two instants of increased water content. It is likely that during the second rainfall event, water from the first event was still infiltrating and during the third event, water from the second event was infiltrating. It is not possible to know with certainty to which rain event the change in slope recorded by the probes in the second ash layer refers. Most probably, all rain events contributed. Finally, in the last ash layer, there was only one instant when the

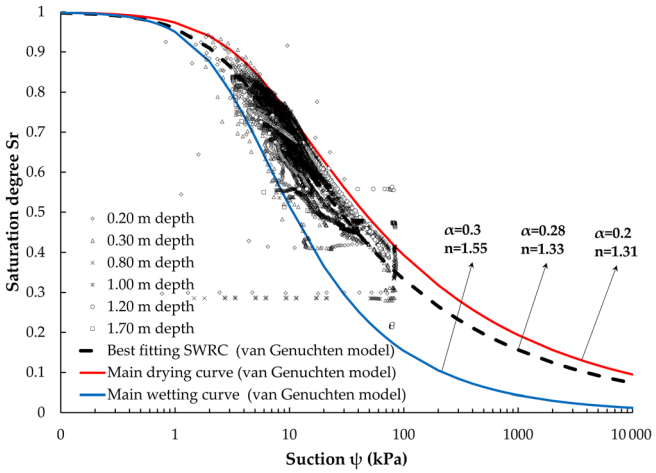

FIGURE 6 Pairs of suction values and degree of saturation curve identified by their interpolation. The graph also shows the main imbibition and drying curves obtained from the laboratory test

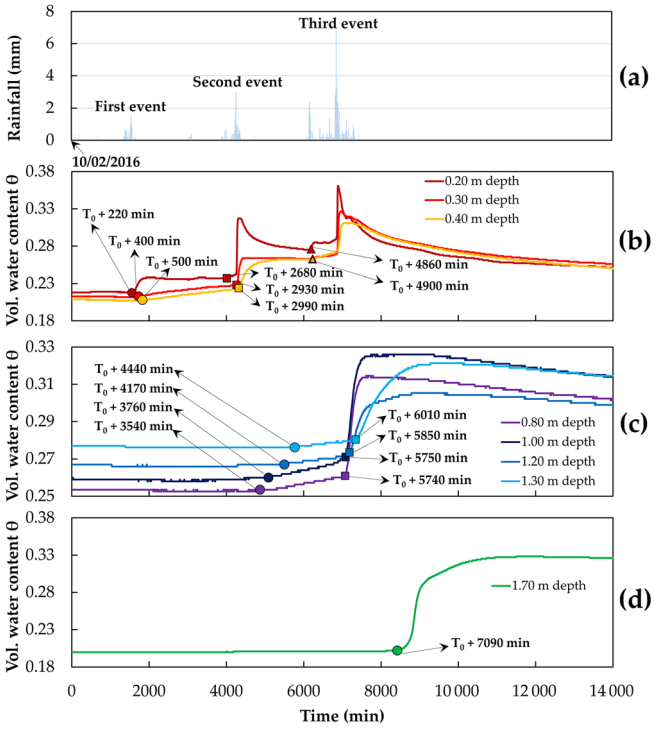

FIGURE 7 (a) Rainfall recorded every 10 min. Period from 10 to 19 February 2016. (b)–(d) Trend of the volumetric water content recorded by the TDR probes at different depths and identification of the instants in which the curves recorded an increase, representative of the arrival of the wet front

curve showed a rapid change in slope. Again, we cannot state with certainty which rainfall event is responsible for the change in water content, so the same considerations apply here as above.

Figure 8 shows the instants identified in Figure 7, in relation to the depth. The times inserted in the graph are equal to the difference between the time identified with respect to the instant of the start of rainfall (T_0). In the figure it is possible to identify the different possible infiltration processes undergone by the soil.

The depth increase/time change ratio indicates the infiltration rate. The steeper the curve, therefore, the faster the infiltration. Regardless of which event contributed to the infiltration process in the deeper layers, it is evident that the infiltration rate recorded in the pumices was much lower than that recorded in the ashes.

Figure 9a shows the rainfall recorded every 10 min for the second period analysed, that is, from 27 February 2016 to 8 March 2016. In this case, the infiltration processes caused by the first two rainfall events, that is, the most significant ones, have been analysed. Figure 9b–d shows the volumetric water content recorded by the TDR probes at different depths. In this case too, the instants in which the curves recorded an increase are highlighted, representative of the arrival of the wet front at that depth. In this case, two changes in the slope of the curves representing the sensors installed in the surface ash layer and only one change in the slope of the curves for the second and third ash layers were highlighted.

Figure 10 shows the instants identified in Figure 9, in relation to the depth. The times inserted in the graph are equal to the difference between the time identified with respect to the instant of the start of rainfall (T_0).

The infiltration relating to this period has a decidedly different behaviour from the first. In this case, the speed with which the water infiltrates the pumice layers is decidedly greater than that recorded in the first case. In the last layer of pumices, it is even higher than the infiltration speed of the ashes.

The last case analysed relates to the period from 21 to 30 April 2016. Figure 11a shows the rainfall recorded every 10 min, where two rainfall events can be distinguished. In actual fact, the first event could be divided into two distinct moments, but since they occurred shortly one after the other, it can be considered as a single event.

Figure 11b–d shows the development of the volumetric water content at different depths. In the graph, two changes in the slope of the curves for the surface ash layer and only one change in the curves for the second and third ash layers can be distinguished. In Figure 12, similarly to the other two events analysed, the instants are shown identified according to depth. As can be seen from the graph, the infiltration behaves in a way very similar to that shown in the first event. In this case too, the infiltration rate in the pumice layers is much lower than that recorded in the ash layers.

3.3 | Soil permeability functions

All the instants identified in the three periods analysed are shown in Table 1. The table also shows the apparent velocities recorded during the events, that is, the ratio between the difference in depth and the difference in time instants ($v = \Delta z/\Delta t$).

The velocities highlighted in grey in the table are those calculated in the pumice layers. Whilst in the ash layers, because the sensors are installed there, it can be said that the trend of the wet front is almost linear, the same cannot be said for the pumice layers. The velocities

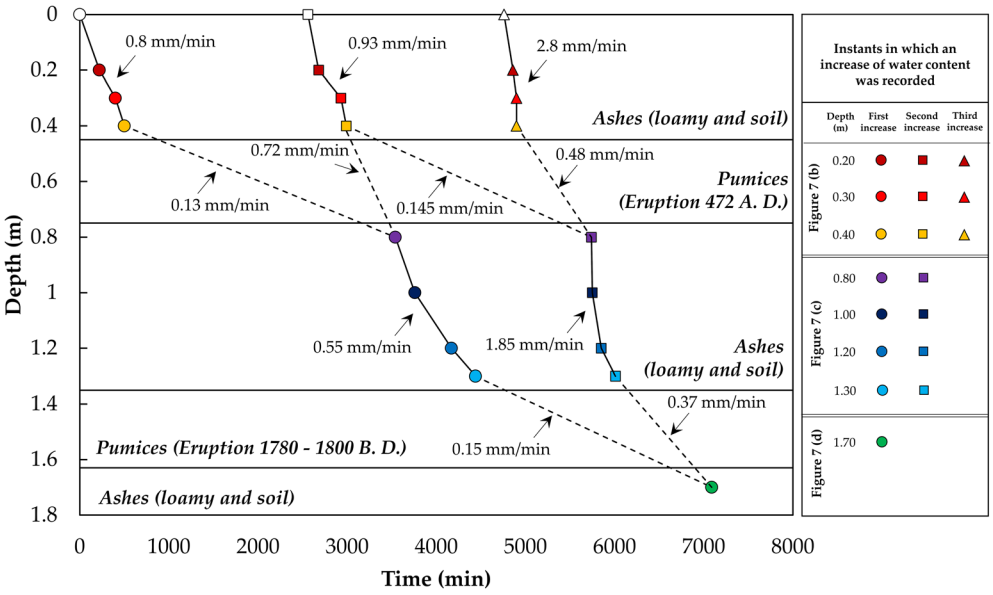

FIGURE 8 Instants at which the curves increased with depth and estimation of the average infiltration velocities in the layers. Period from 10 to 19 February 2016

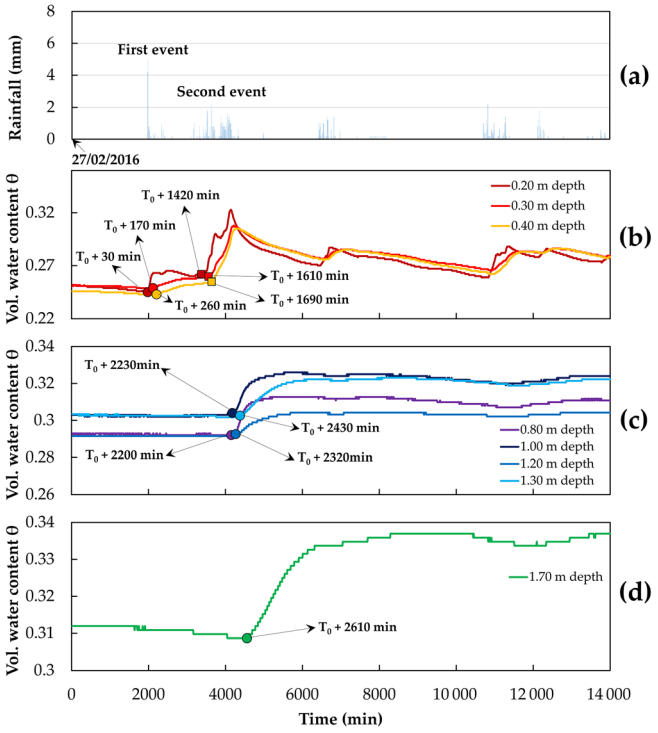

FIGURE 9 (a) Rainfall recorded every 10 min. Period from 27 February 2016 to 8 March 2016. (b)–(d) Trend of the volumetric water content recorded by the TDR probes at different depths and identification of the instants in which the curves recorded an increase, representative of the arrival of the wet front

for the pumice layers are average velocities, but there is no indication of the trend with respect to depth. In fact, according to some studies, the trend in this layer is decidedly nonlinear. For example, in Capparelli et al. (2020), in an experimental test carried out with a physical model in which a deposit with a stratigraphy similar to the monitored slope was reconstructed, moisture sensors were also inserted in the pumice layer, which made it possible to identify the instants of arrival of the wet front. In this case it was shown that the velocity profile in the pumice layer is nonlinear. In particular, the velocity is very low in the initial part, and then increases as the depth increases (Figure 13).

Using the apparent infiltration velocities, an attempt was made to determine the permeability coefficients.

Table 2 shows the values of the permeability coefficient calculated in the ash layers for all the events of the three periods analysed. In order to determine the permeability coefficients, in addition to the velocity values defined in Table 1, the suction values recorded by the tensiometers at the different depths at the start of the event were identified. In addition, the water content values recorded by the TDR probes at the start of the event were also identified and included.

The k-ψ and k-θ value pairs were diagrammed in order to define the soil permeability functions $k(\psi)$ and $k(\theta)$. The pairs were interpolated with the hydraulic conductivity function model of van Genuchten–Mualem.

The calibration parameters of the model are given in Table 3.

As can be seen from Figure 14, the data do not align perfectly with the interpolation curves. Since the permeability coefficient is a parameter with great variability (even several orders of magnitude) and is very susceptible to localised conditions, this behaviour was to be expected. Moreover, since the data used refer to limited variations in water content (and therefore suction), it is difficult to interpolate the curve as well as possible.

4 | DISCUSSION

4.1 | The role of pumices as a capillary barrier

Historically, infiltration processes in unsaturated porous media have been developed by Richards (1931), which also extended Darcy's law to motion in unsaturated media. According to this approach, in a

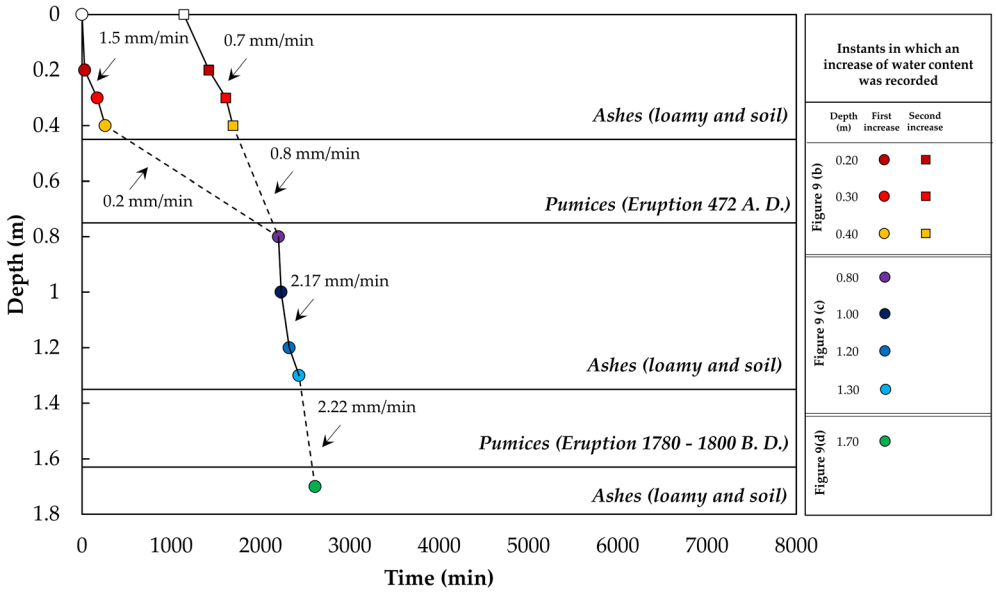

FIGURE 10 Instants when the curves increased with respect to depth and estimation of the average infiltration velocities in the layers. Period from 27 February 2016 to 8 March 2016

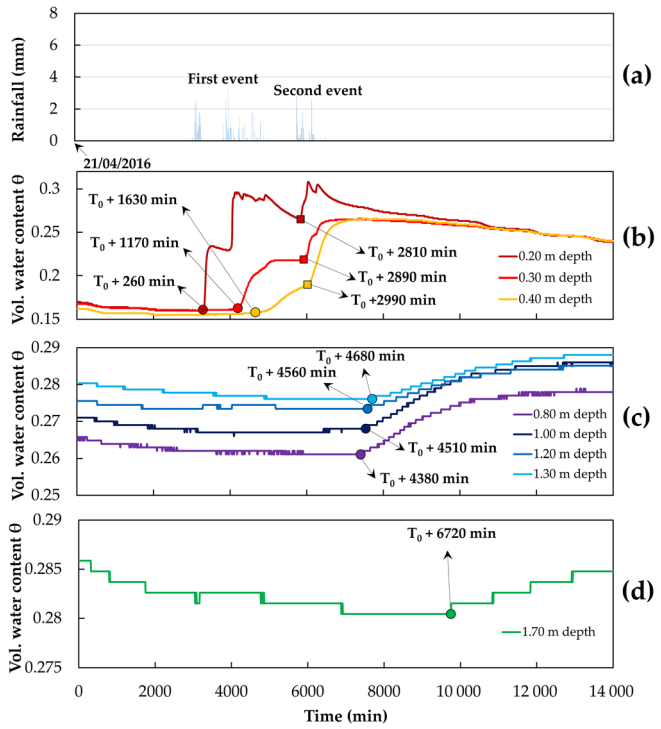

FIGURE 11 (a) Rainfall recorded every 10 min. Period from 21 to 30 April 2016. (b)–(d) Trend of the volumetric water content recorded by the TDR probes at different depths and identification of the instants in which the curves recorded an increase, representative of the arrival of the wet front

three-phase medium, hydraulic conductivity is reduced and depends on the local values of water content. The proportionality factor k of Darcy's law becomes a function of the total potential and of the volumetric water content θ. Therefore, according to Richards' schematization, if Darcy's law is combined with the continuity equation, an equation is obtained which it is possible to describe the flow of water in a homogeneous saturated or partially saturated soil. The infiltration is affected by the intensity and duration of the rainfall, the permeability characteristics of the soil and the tensional state and initial water content of the soil.

In the case of stratified deposits, however, other phenomena also occur, especially at the interface between two granulometrically different layers. In the case of fine soils placed on top of coarse soils, downward infiltration disturbances may occur. The fine material, due to the surface tension, tends to retain water, preventing it from passing into the lower layer. Some authors (Khire et al., 2000; Mancarella & Simeone, 2012; Tidwell et al., 2003) call the phenomenon a "capillary barrier". Pumices, on the other hand, have their own unsaturated conductivity (which at high suction can be much lower than that of ashes) and a suitable gradient needs to be established for a certain flow rate to be able to infiltrate. The concept of "capillary barrier" therefore simplifies all the phenomena that occur at the interface of the two granulometrically different layers that cause disturbances to infiltration.

The coarser material, due to its lower conductivity and lower water retention in unsaturated conditions, can in fact hinder, or even temporarily prevent, the infiltration process from spreading to the lower layer. The hydraulic conductivity of pumices is very low for high suction values (in almost dry conditions) and then increases rapidly as the degree of saturation increases. It follows that the time-depth ratio characteristic of a stratified deposit such as the one under examination has a highly variable form. The speed at which water infiltrates the pumice is strongly affected by the state of tension and the initial conditions of water content.

In the case under examination, therefore, the infiltration at right angles to the surface of the slope relative to the first period analysed, underwent a stop until a gradient was established that overcame the hydraulic impedance of the unsaturated conductivity of the pumice. To make an analogy with the simplification of the "capillary barrier", it can be said that the infiltration at right angles to the surface of the

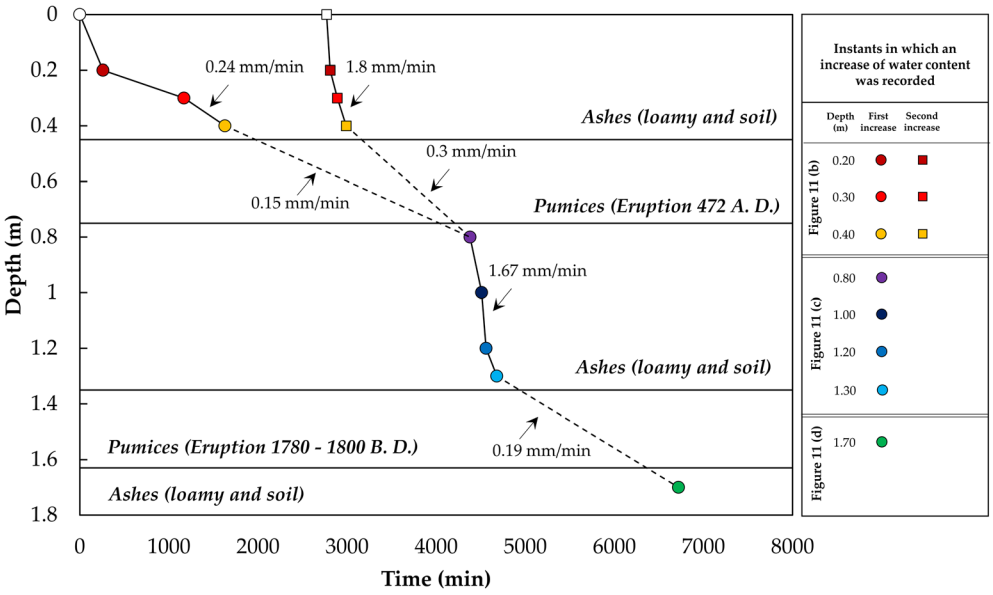

FIGURE 12 Instants at which the curves recorded an increase in relation to the depth and estimation of the average infiltration velocities in the layers. Period from 21 to 30 April 2016

TABLE 1 Instants of arrival of the wet front identified in the three periods analysed and their apparent infiltration velocities. Highlighted in grey are the average velocities calculated in the pumice layers

	Soil	Depth	Rain arrival time			$v = \Delta z/\Delta t$		
			February	February–March	April	February	February–March	April
		(m)	(min)	(min)	(min)	(m/s)	(m/s)	(m/s)
First event	G.L.	0.0	1330	1950	3030			
	B	0.2	1550	1980	3290	1.52×10^{-05}	1.11×10^{-04}	1.28×10^{-05}
		0.3	1730	2120	4200	9.26×10^{-06}	1.19×10^{-05}	1.83×10^{-06}
		0.4	1830	2210	4660	1.67×10^{-05}	1.85×10^{-05}	3.62×10^{-06}
	Bb	0.8	4870	4150	7410	2.19×10^{-06}	3.44×10^{-06}	2.42×10^{-06}
		1.0	5090	4180	7540	1.52×10^{-05}	1.11×10^{-04}	2.56×10^{-05}
		1.2	5500	4270	7590	8.13×10^{-06}	3.70×10^{-05}	6.67×10^{-05}
		1.3	5770	4380	7710	6.17×10^{-06}	1.52×10^{-05}	1.39×10^{-05}
	2Bb	1.7	8420	4560	9750	2.52×10^{-06}	3.70×10^{-05}	3.27×10^{-06}
Second event	G.L.	0.0	3890	3090	0			
	B	0.2	4010	3370	5840	2.78×10^{-05}	1.19×10^{-05}	5.71×10^{-07}
		0.3	4260	3560	5920	6.67×10^{-06}	8.77×10^{-06}	2.08×10^{-05}
		0.4	4320	3640	6020	2.78×10^{-05}	2.08×10^{-05}	1.67×10^{-05}
	Bb	0.8	7070	4150	7410	2.42×10^{-06}	1.31×10^{-05}	4.80×10^{-06}
		1.0	7080	4180	7540	3.33×10^{-04}	1.11×10^{-04}	2.56×10^{-05}
		1.2	7180	4270	7590	3.33×10^{-05}	3.70×10^{-05}	6.67×10^{-05}
		1.3	7340	4380	7710	1.04×10^{-05}	1.52×10^{-05}	1.39×10^{-05}
	2Bb	1.7	8420	4560	9750	6.17×10^{-06}	3.70×10^{-05}	3.27×10^{-06}
Third event	G.L.	0.0	6090					
	B	0.2	6190			3.33×10^{-05}		
		0.3	6230			4.17×10^{-05}		
		0.4	6231			1.67×10^{-03}		
	Bb	0.8	7070			7.95×10^{-06}		
		1.0	7080			3.33×10^{-04}		
		1.2	7180			3.33×10^{-05}		
		1.3	7340			1.04×10^{-05}		
	2Bb	1.7	8420			6.17×10^{-06}		

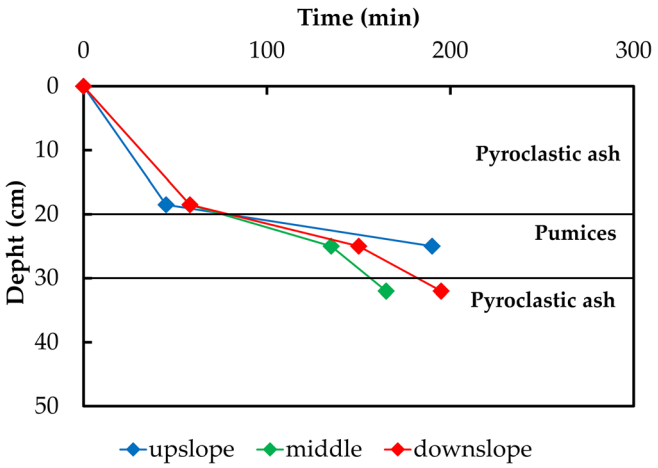

FIGURE 13 Arrival times of the wet front at various depths in the investigated alignments onset of soil moisture variation as detected by TDR probes (modified after Capparelli et al., 2020)

slope (Figure 15a), stopped at the interface between the layers (Figure 15b), until the water pressure reached values such as to "break the barrier" and therefore continue in the underlying layer of pumice (Figure 15c).

In these cases, the hydraulic impedance forces the upper layer to accumulate more water, favouring the saturation of the upper layers, affecting the infiltration processes and conditioning the stability of the slope.

4.2 | The temporal variability of infiltration processes

In the second period analysed, infiltration into the different soil layers was much more linear. In this case, the pumices did not obstruct the passage of water. In fact, considering the infiltration rates, it can be said that they even favoured it. The rainfall events of the second period occurred only a few weeks after those of the first. The February rainfall affected the moisture conditions in the pumice, increasing the water content in the layer. In this configuration, the hydraulic conductivity of the pumices increased greatly, which facilitated the passage of water to the deeper ash layers.

In the last period analysed, behaviour very similar to that recorded in the first period was recorded. Again, the pumices hindered infiltration. The time-depth curve for these layers had a much steeper slope than that of the ash. The pumices had reverted to a much drier condition with a relative decrease in the permeability coefficient.

This is even more evident if one considers the initial conditions of the moisture profiles in the three periods analysed (Figure 16). From the illustration, it is evident that the soil, before the rainfall events recorded between February and March, had a higher water content than during the other two events analysed. The sensors, however, are only installed in the ash layers, so we are not certain of the moisture conditions of the pumice, but it is presumable and highly likely that a higher water content exists when this is greater in the two layers that pack it.

In addition to the duration and intensity of the rainfall, infiltration is therefore strongly influenced by the initial conditions of water content of the pumice layers.

The Figures 8, 10 and 12 show that in ash, the curves have a much less variable slope than in pumice. Infiltration processes in ash are also affected by initial soil moisture conditions and the characteristics of rainfall events, but this effect is much more pronounced in pumice layers. The dry conditions of the pumice layers may therefore hinder drainage in the lower layers, thus favouring the rapid accumulation of water within the canopy during rainfall events, which may eventually lead to slope failure.

However, it must be considered that the dry conditions of the pumice hinder water drainage only for a limited time. The persistence of the diverted flow for a longer time would be favoured by a dryer initial condition and by a very high rainfall intensity and although rainfall events with high intensity are not rare, they mostly occur when the soil is already wet (Capparelli et al., 2020).

A long-lasting capillary barrier with associated diverted flow component could be guaranteed by very dry initial conditions, and by the extremely different hydraulic characteristic curves of the two soils (Mancarella & Simeone, 2012).

The data we analysed showed that the capillary barrier occurred, but it did not lead to instability. There were no very dry soil conditions associated with very heavy rainfall. Whilst it cannot be completely ruled out that these conditions may occur, they are extremely rare events.

Although the concept of the capillary barrier has already been extensively discussed in other studies, this work demonstrates that the phenomenon is extremely variable. In the same analysis site, with the same soils and textures, it is possible that it occurs or not depending on the previous rains and therefore on the initial humidity conditions.

There are innumerable combinations of humidity initial conditions and precipitations that can favour or hinder the formation of the capillary barrier. With in situ data it is difficult to categorise all these combinations and therefore it is difficult to identify threshold combinations that may or may not induce the formation of the barrier. Therefore, this is a still open topic that can be faced and analysed with laboratory tests that are better suited to a categorisation of events, as it is possible to easily impose different conditions. It is therefore the authors' intention to expand the experimentation on this topic in order to offer an increasingly complete picture of the dynamics of these phenomena.

5 | CONCLUSIONS

The process of rainfall infiltration in a stratified volcanoclastic slope located in Sarno, southern Italy, near the Vesuvius volcano, was analysed. Specifically, the slope is formed by alternating volcanic ash

TABLE 2 Suction values and water content recorded at different depths at the start of the event and calculation of permeability coefficients

	Event start	Depth	$v = \Delta z/\Delta t$	Water content	Suction		$\Delta\psi/\Delta z$	$k = v/(1-\Delta\psi/\Delta z)$
	(min)	(m)	(m/s)	(m^3/m^3)	(kPa)	(m)	(m/m)	(m/s)
February	1330	0.2		0.22	12.3	1.26		
		0.3	9.26×10^{-06}	0.21	11.5	1.17	−0.86	4.99×10^{-06}
		0.8		0.25	11.0	1.12		
		1.0	1.52×10^{-05}	0.26	10.1	1.03	−0.44	1.05×10^{-05}
		1.2	8.13×10^{-06}	0.27	9.2	0.94	−0.44	5.63×10^{-06}
	3890	0.2		0.24	7.3	0.75		
		0.3	6.67×10^{-06}	0.23	8.2	0.84	0.93	8.91×10^{-05}
		0.8		0.25	11.0	1.12		
		1.0	1.52×10^{-05}	0.26	10.1	1.03	−0.47	1.03×10^{-05}
		1.2	8.13×10^{-06}	0.27	9.3	0.95	−0.40	5.82×10^{-06}
	6090	0.2		0.28	5.7	0.59		
		0.3	4.17×10^{-05}	0.26	5.4	0.55	−0.33	3.13×10^{-05}
		0.8		0.26	9.4	0.96		
		1.0	3.33×10^{-04}	0.26	8.8	0.90	−0.28	2.60×10^{-04}
		1.2	3.33×10^{-05}	0.27	8.5	0.87	−0.15	2.90×10^{-05}
February–March	1950	0.2		0.25	8.8	0.90		
		0.3	1.19×10^{-05}	0.25	8.2	0.84	−0.61	7.39×10^{-06}
		0.8		0.29	9.0	0.91		
		1.0	1.11×10^{-04}	0.30	8.2	0.83	−0.40	7.92×10^{-05}
		1.2	3.70×10^{-05}	0.29	7.5	0.76	−0.36	2.72×10^{-05}
	3090	0.2		0.26	6.8	0.69		
		0.3	8.77×10^{-06}	0.26	7.0	0.72	0.21	1.11×10^{-05}
		0.8		0.29	9.0	0.91		
		1.0	1.52×10^{-05}	0.30	8.2	0.83	−0.40	1.08×10^{-05}
		1.2	8.13×10^{-06}	0.29	7.5	0.76	−0.35	6.01×10^{-06}
April	3030	0.2		0.16	26.9	2.74		
		0.3	1.83×10^{-06}	0.16	21.0	2.15	−5.97	2.63×10^{-07}
		0.8		0.26	13.6	1.39		
		1.0	2.56×10^{-05}	0.27	12.6	1.29	−0.52	1.69×10^{-05}
		1.2	6.67×10^{-05}	0.27	11.7	1.19	−0.49	4.46×10^{-05}
	5800	0.2		0.29	6.5	0.66		
		0.3	2.08×10^{-05}	0.22	6.9	0.70	0.36	3.25×10^{-05}
		0.8		0.26	13.7	1.40		
		1.0	1.52×10^{-05}	0.27	12.7	1.29	−0.54	9.83×10^{-06}
		1.2	8.13×10^{-06}	0.27	11.7	1.19	−0.53	5.33×10^{-06}

TABLE 3 Calibration parameters of the van Genuchten–Mualem model

k_{sat} (m/s)	α (kPa^{-1})	n	m
5×10^{-4}	0.28	6	0.83

(silty-sandy–clayey palaeosoils) interspersed with pumice (sandy-gravelly), due to the different eruptive phases of the volcanic complexes in the area. A monitoring station consisting of a rain gauge, seven tensiometers and eight TDR probes was installed on this slope to measure rainfall intensity, suction ψ and volumetric water content θ, respectively. The data recorded by the station made it possible to define the average water retention curve for pyroclastic ash. Furthermore, in order to understand the evolution of the infiltration process into the ground, three significant rainfall periods were isolated and analysed. The rainfall periods identified relate to the month of February, between February and March and the month of April. For each of these periods, the volumetric water content recorded by the

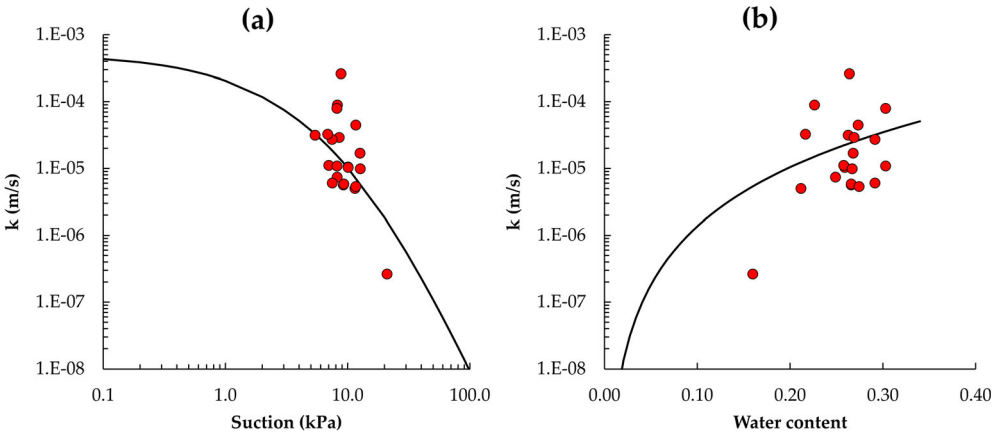

FIGURE 14 (a) Pairs of k-ψ values and interpolation with the van Genuchten–Mualem model. (b) Pairs of k-θ values and interpolation with the van Genuchten–Mualem model

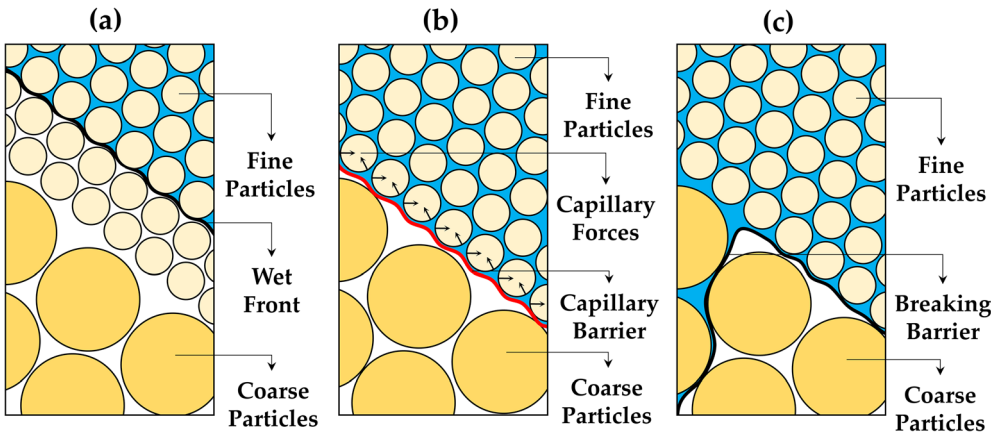

FIGURE 15 Schematisation of the "capillary barrier" phenomenon. (a) Vertical infiltration, (b) capillary barrier, (c) break of barrier

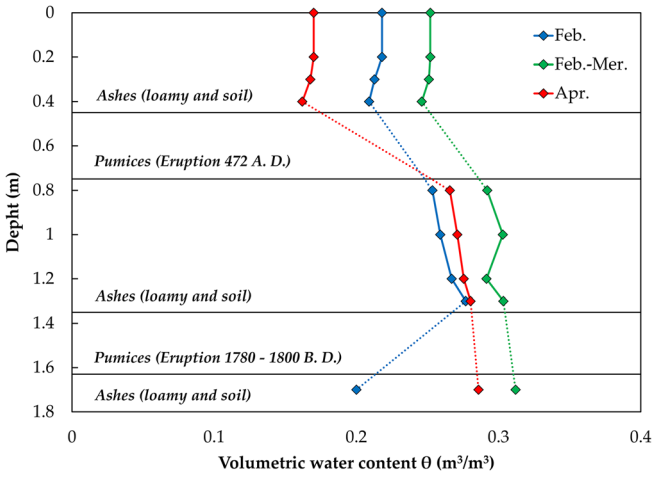

FIGURE 16 Initial conditions of volumetric soil water content before the analysed events

TDR probes at the various depths was plotted and the time in which they were affected by the arrival of the wet front, that is, the instant in which the curve showed a rapid increase, was identified. These instants were related to the depth of installation of the sensor, thus defining the speed at which the water infiltrated, and using these figures, the relationships between the permeability coefficient with the volumetric water content and suction were defined. The soil water retention curve and the hydraulic conductivity function of the soil, both defined experimentally, can be used in numerical models that simulate the evolution of infiltration in soils with the same hydraulic and textural characteristics. In the first and third periods analysed, the pumices hindered the infiltration process. This was due to the very low unsaturated conductivity of the dry pumices, which required the formation of a high pressure gradient for water to penetrate through them. In the second period, however, because the pumice layers were wetter, the hydraulic conductivity was much higher, favouring infiltration. The results obtained indicate that coarse pumice layers, when they have a low water content, delay the advancement of the wet front, inducing the accumulation of water in the overlying ashes. Conversely, when they are wet, they can even promote the passage of water into the underlying ash layer.

In addition to the duration and intensity of rainfall, infiltration is therefore strongly influenced by the initial conditions of water content of the pumice layers. In the ashes too, the infiltration processes are influenced by the initial soil moisture conditions and the characteristics of the rainfall events, but this influence is much more pronounced in the pumice layers. Dry conditions in the pumice layers may therefore hinder drainage in the lower layers, thus favouring the rapid accumulation of water inside the covering during rainfall events.

ACKNOWLEDGEMENTS

The authors gratefully acknowledge the financial support provided by the framework of the SILA—PONa3_00341 project An Integrated System of Laboratories for the Environment. Open Access Funding provided by Universita della Calabria within the CRUI-CARE Agreement.

DATA AVAILABILITY STATEMENT

Data sharing is not applicable to this article as no new data were created or analyzed in this study.

ORCID

Giovanna Capparelli https://orcid.org/0000-0003-3324-8224
Gennaro Spolverino https://orcid.org/0000-0002-5637-5384

REFERENCES

Basile, A., Mele, G., & Terribile, F. (2003). Soil hydraulic behaviour of a selected benchmark soil involved in the landslide of Sarno 1998. *Geoderma*, *117*, 331–346. https://doi.org/10.1016/S0016-7061(03)00132-0

Baum, R. L., Godt, J. W., & Savage, W. Z. (2010). Estimating the timing and location of shallow rainfall-induced landslides using a model for transient, unsaturated infiltration. *Journal of Geophysical Research*, *115*, F03013. https://doi.org/10.1029/2009JF001321

Bogaard, T. A., & Greco, R. (2016). Landslide hydrology: From hydrology to pore pressure. *WIREs Water*, *3*(3), 439–459. https://doi.org/10.1002/wat2.1126

Brooks, R.H., & Corey, A.T. (1964). Hydraulic properties of porous media (Hydrology paper 3) Colorado State University.

Capparelli, G., Damiano, E., Greco, R., Olivares, L., & Spolverino, G. (2020). Physical modeling investigation of rainfall infiltration in steep layered volcanoclastic slopes. *Journal of Hydrology*, *580*, 124199. https://doi.org/10.1016/j.jhydrol.2019.124199

Capparelli, G., & Spolverino, G. (2020). An empirical approach for modeling hysteresis behavior of pyroclastic soils. *Hydrology*, *7*, 14. https://doi.org/10.3390/hydrology7010014

Capparelli, G., Spolverino, G., & Greco, R. (2018). Experimental determination of TDR calibration relationship for pyroclastic ashes of Campania (Italy). *Sensors*, *18*, 3727. https://doi.org/10.3390/s18113727

Cascini, L., Cuomo, S., & Guida, D. (2008). Typical source areas of may 1998 flow-like mass movements in the Campania region, southern Italy. *Engineering Geology*, *96*, 107–125. https://doi.org/10.1016/j.enggeo.2007.10.003

Cascini, L., Ferlisi, S., & Vitolo, E. (2008). Individual and societal risk owing to landslides in the Campania region (southern Italy). *Georisk: Assessment and Management of Risk for Engineered Systems and Geohazards*, *2*(3), 125–140. https://doi.org/10.1080/17499510802291310

Cascini, L., Sorbino, G., Cuomo, S., & Ferlisi, S. (2014). Seasonal effects of rainfall on the shallow pyroclastic deposits of the Campania region (southern Italy). *Landslides*, *11*, 779–792. https://doi.org/10.1007/s10346-013-0395-3

Collins, B. D., & Znidarcic, D. (2004). Stability analyses of rainfall induced landslides. *Journal of Geotechnical and Geoenvironmental Engineering*, *130*(4), 362–372. https://doi.org/10.1061/(ASCE)1090-0241(2004)130:4(362)

Comegna, L., Damiano, E., Greco, R., Guida, A., Olivares, L., & Picarelli, L. (2016). Field hydrological monitoring of a sloping shallow pyroclastic deposit. *Canadian Geotechnical Journal*, *53*(7), 1125–1137. https://doi.org/10.1139/cgj-2015-0344

Damiano, E., Greco, R., Guida, A., Olivares, L., & Picarelli, L. (2017). Investigation on rainwater infiltration into layered shallow covers in pyroclastic soils and its effect on slope stability. *Engineering Geology*, *220*, 208–218. https://doi.org/10.1016/j.enggeo.2017.02.006

Damiano, E., & Olivares, L. (2010). The role of infiltration processes in steep slope stability of pyroclastic granular soils: Laboratory and numerical investigation. *Natural Hazards*, *52*(2), 329–350. https://doi.org/10.1007/s11069-009-9374-3

de Luca, D. L., & Capparelli, G. (2022). Rainfall nowcasting model for early warning systems applied to a case over central Italy. *Natural Hazards*, *112*, 501–520. https://doi.org/10.1007/s11069-021-05191-w

de Vita, P., Agrello, D., & Ambrosino, F. (2006). Landslide susceptibility assessment in ashfall pyroclastic deposits surrounding mount Somma-Vesuvius. Application of geophysical surveys for soil thickness mapping. *Journal of Applied Geophysics*, *59*, 126–139. https://doi.org/10.1016/j.jappgeo.2005.09.001

de Vita, P., Fusco, F., Tufano, R., & Cusano, D. (2018). Seasonal and event-based hydrological and slope stability modeling of pyroclastic fall deposits covering slopes in Campania (southern Italy). *Water*, *10*, 1140. https://doi.org/10.3390/w10091140

de Vita, P., Napolitano, E., Godt, J., & Baum, R. (2013). Deterministic estimation of hydrological thresholds for shallow landslide initiation and slope stability models: Case study from the Somma-Vesuvius area of southern Italy. *Landslides*, *10*, 713–728. https://doi.org/10.1007/s10346-012-0348-2

del Prete, M., Guadagno, F. M., & Hawkins, A. B. (1998). Preliminary report on the landslides of 5 may 1998, Campania, southern Italy. *Bulletin of Engineering Geology and the Environment*, *57*, 113–129. https://doi.org/10.1007/s100640050028

del Soldato, M., Pazzi, V., Segoni, S., De Vita, P., Tofani, V., & Moretti, S. (2018). Spatial modeling of pyroclastic cover deposit thickness (depth to bedrock) in peri-volcanic area of Campania (southern Italy). *Earth Surface Processes and Landforms*, *43*, 1757–1767. https://doi.org/10.1002/esp.4350

di Crescenzo, G., & Santo, A. (2005). Debris slides–rapid earth flows in the carbonate massifs of the Campania region (southern Italy): Morphological and morphometric data for evaluating triggering susceptibility. *Geomorphology*, *66*, 255–276. https://doi.org/10.1016/j.geomorph.2004.09.015

di Martire, D., De Rosa, M., Pesce, V., Santangelo, M. A., & Calcaterra, D. (2012). Landslide hazard and land management in high-density urban areas of Campania region, Italy. *Natural Hazards and Earth System Sciences*, *12*, 905–926. https://doi.org/10.5194/nhess-12-905-2012

Formetta, G., & Capparelli, G. (2019). Quantifying the three-dimensional effects of anisotropic soil horizons on hillslope hydrology and stability. *Journal of Hydrology*, *570*, 329–342. https://doi.org/10.1016/j.jhydrol.2018.12.064

Fredlund, D. G., & Morgenstern, N. R. (1977). Stress state variables for unsaturated soils. *Journal of the Geotechnical Engineering Division*, *103*, 447–466. https://doi.org/10.1061/AJGEB6.0000423

Greco, R., Comegna, L., Damiano, E., Guida, A., Olivares, L., & Picarelli, L. (2013). Hydrological modelling of a slope covered with shallow pyroclastic deposits from field monitoring data. *Hydrology and Earth System Sciences*, *17*, 4001–4013. https://doi.org/10.5194/hess-17-4001-2013

Greco, R., & Gargano, R. (2015). A novel equation for determining the suction stress of unsaturated soils from the water retention curve based on wetted surface area in pores. *Water Resources Research*, *51*, 6143–6155. https://doi.org/10.1002/2014WR016541

Hübner, R., Günther, T., Heller, K., Noell, U., & Kleber, A. (2017). Impacts of a capillary barrier on infiltration and subsurface stormflow in layered slope deposits monitored with 3-D ERT and hydrometric measurements. *Hydrology and Earth System Sciences*, *21*, 5181–5199. https://doi.org/10.5194/hess-21-5181-2017

Jones, S. B., Wraith, J. M., & Or, D. (2002). Time domain reflectometry measurement principles and applications. *Hydrological Processes*, *16*, 141–153. https://doi.org/10.1002/hyp.513

Khire, M. V., Benson, C. H., & Bosscher, P. J. (2000). Capillary barriers: Design variables and water balance. *Journal of Geotechnical and*

Geoenvironmental Engineering, *126*, 695–708. https://doi.org/10.1061/(ASCE)1090-0241(2000)126:8(695)

Lu, N., & Godt, J. W. (2008). Infinite slope stability under steady unsaturated seepage conditions. *Water Resources Research*, *44*, W11404. https://doi.org/10.1029/2008WR006976

Lu, N., Godt, J. W., & Wu, D. T. (2010). A closed-form equation for effective stress in unsaturated soil. *Water Resources Research*, *46*, W05515. https://doi.org/10.1029/2009WR008646

Lu, N., Kaya, B. S., & Godt, J. W. (2011). Direction of unsaturated flow in a homogeneous and isotropic hillslope. *Water Resources Research*, *47*, W02519. https://doi.org/10.1029/2010WR010003

Lv, H., Ling, C., Hu, B. X., Ran, J., Zheng, Y., Xu, Q., & Tong, J. (2019). Characterizing groundwater flow in a translational rock landslide of southwestern China. *Bulletin of Engineering Geology and the Environment*, *78*, 1989–2007. https://doi.org/10.1007/s10064-017-1212-3

Mancarella, D., Doglioni, A., & Simeone, V. (2012). On capillary barrier effects and debris slide triggering in unsaturated soil covers. *Engineering Geology*, *147–148*, 14–27. https://doi.org/10.1016/j.enggeo.2012.07.003

Mancarella, D., & Simeone, V. (2012). Capillary barrier effects in unsaturated layered soils, with special reference to the pyroclastic veneer of the Pizzo d'Alvano, Campania. Italy. *Bulletin of Engineering Geology and the Environment*, *71*, 791–801. https://doi.org/10.1007/s10064-012-0419-6

Olivares, L., Damiano, E., Netti, N., & De Cristofaro, M. (2019). Geotechnical properties of two pyroclastic deposits involved in catastrophic flowslides for implementation in early warning systems. *Geosciences*, *9*(1), 24. https://doi.org/10.3390/geosciences9010024

Padilla, C., Onda, Y., Iida, T., Takahashia, S., & Uchidab, T. (2014). Characterization of the groundwater response to rainfall on a hillslope with fractured bedrock by creep deformation and its implication for the generation of deep-seated landslides on Mt. Wanitsuka, Kyushu Island. *Geomorphology*, *204*, 444–458. https://doi.org/10.1016/j.geomorph.2013.08.024

Revellino, P., Guadagno, F. M., & Hungr, O. (2008). Morphological methods and dynamic modelling in landslide hazard assessment of the Campania Apennine carbonate slope. *Landslides*, *5*, 59–70. https://doi.org/10.1007/s10346-007-0103-2

Richards, L. A. (1931). Capillary conduction of liquids through porous mediums. *Journal of Applied Physics*, *1*(5), 318–333. https://doi.org/10.1063/1.1745010

Rolandi, G., Bellucci, F., Heizler, M. T., Belkin, H. E., & De Vivo, B. (2003). Tectonic controls on the genesis of ignimbrites from the Campanian volcanic zone, southern Italy. *Mineralogy and Petrology*, *79*, 3–31. https://doi.org/10.1007/s00710-003-0014-4

Ross, B. (1990). The diversion capacity of capillary barriers. *Water Resources Research*, *26*(10), 2625–2629. https://doi.org/10.1029/WR026i010p02625

Schneider, P., Pool, S., Strouhal, L., & Seibert, J. (2014). True colors – Experimental identification of hydrological processes at a hillslope prone to slide. *Hydrology and Earth System Sciences*, *18*, 875–892. https://doi.org/10.5194/hess-18-875-2014

Sorbino, G., & Nicotera, M. V. (2013). Unsaturated soil mechanics in rainfall-induced flow landslides. *Engineering Geology*, *165*, 105–135. https://doi.org/10.1016/j.enggeo.2012.10.008

Spolverino, G., Capparelli, G., & Versace, P. (2019). An instrumented flume for infiltration process modeling, landslide triggering and propagation. *Geosciences*, *9*(3), 108. https://doi.org/10.3390/geosciences9030108

Stormont, J. C., & Anderson, C. E. (1999). Capillary barrier effect from underlying coarser soil layer. *Journal of Geotechnical and Geoenvironmental Engineering*, *125*(8), 641–648. https://doi.org/10.1061/(ASCE)1090-0241(1999)125:8(641)

Tidwell, V. C., Glass, R. J., Chocas, C., Barker, G., & Orear, L. (2003). Visualization experiment to investigate capillary barrier performance in the context of a Yucca Mountain emplacement drift. *Journal of Contaminant Hydrology*, *62*(3), 287–301. https://doi.org/10.1016/S0169-7722(02)00164-X

Topp, G. C., Davis, J. L., & Annan, A. P. (1980). Electromagnetic determination of soil water content: Measurement in coaxial transmission lines. *Water Resources Research*, *16*, 574–582. https://doi.org/10.1029/WR016i003p00574

van Genuchten, M. T. (1980). A closed form equation for predicting the hydraulic conductivity of unsaturated soils. *Soil Science Society of America Journal*, *44*, 892–898. https://doi.org/10.2136/sssaj1980.03615995004400050002x

Vanapalli, S. K., Fredlund, D. G., Pufahl, D. E., & Clifton, A. W. (1996). Model for the prediction of shear strength with respect to soil suction. *Canadian Geotechnical Journal*, *33*(3), 379–392. https://doi.org/10.1139/t96-060

von Ruette, J., Lehmann, P., & Or, D. (2014). Effects of rainfall spatial variability and intermittency on shallow landslide triggering patterns at a catchment scale. *Water Resources Research*, *50*, 7780–7799. https://doi.org/10.1002/2013WR015122

Warrick, A. W., Wierenga, P. J., & Pan, L. (1997). Downward water flow through sloping layers in the vadose zone: Analytical solutions for diversions. *Journal of Hydrology*, *192*, 321–337. https://doi.org/10.1016/S0022-1694(96)03080-6

Wheeler, S. J., Sharma, R. S., & Buisson, M. S. R. (2003). Coupling of hydraulic hysteresis and stress–strain behaviour in unsaturated soils. *Géotechnique*, *53*, 41–54. https://doi.org/10.1680/geot.2003.53.1.41

Wieczorek, G. F., & Glade, T. (2005). Climatic factors influencing occurrence of debris flows. In *Debris-flow hazards and related phenomena* (pp. 325–362). Springer Praxis Books, Springer. https://doi.org/10.1007/3-540-27129-5_14

Yang, H., Rahardjo, H., & Leong, E. C. (2006). Behavior of unsaturated layered soil columns during infiltration. *Journal of Hydrologic Engineering*, *11*(4), 329–337. https://doi.org/10.1061/(ASCE)1084-0699(2006)11:4(329)

How to cite this article: Capparelli, G., & Spolverino, G. (2022). Hydrological monitoring of a slope covered by stratified pyroclastic deposits and analysis of infiltration processes. *Hydrological Processes*, *36*(6), e14634. https://doi.org/10.1002/hyp.14634